Ablation and associated energy balance of a horizontal glacier surface on Kilimanjaro

Thomas Mölg

Tropical Glaciology Group, Department of Geography, Innsbruck University Network of Climate and Cryospheric Research, University of Innsbruck, Innsbruck, Austria

Douglas R. Hardy

Climate System Research Center, Department of Geosciences, University of Massachusetts, Amherst, Massachusetts, USA

Received 7 November 2003; revised 30 March 2004; accepted 9 June 2004; published 25 August 2004.

[1] The surface energy balance of a glacier describes the physical connection between ice/snow ablation and climatic forcing. To expand knowledge on the response of Kilimanjaro's glaciers to climate variations, this study estimates the energy balance on a horizontal glacier surface at the summit for the periods March to September 2000 and March 2001 to February 2002. An automatic weather station (AWS) operating at 5794 m above sea level provides the data input, and ablation at the AWS site differed considerably between the two periods. The energy balance model employed incorporates radiative fluxes, turbulent heat fluxes, and the energy flux in the subsurface. On a monthly basis, results show that radiative energy dominates energy exchanges at the glacier-atmosphere interface, governed by the variation in net shortwave radiation. The turbulent latent heat flux, which is always negative (i.e., continuous mass loss due to sublimation), is the second important energy flux. In contrast, turbulent exchange of sensible heat remains of minor importance. The marked difference in ablation between the two periods can largely be explained by a difference in surface albedo. Albedo depends on precipitation amount and frequency and directly controls net shortwave radiation receipt. In the context of modern glacier retreat on Kilimanjaro the results support other evidence that Kilimanjaro's glaciers are extremely sensitive to precipitation variability. *INDEX TERMS:* 1827 Hydrology: Glaciology (1863); 3307 Meteorology and Atmospheric Dynamics: Boundary layer processes; 3309 Meteorology and Atmospheric Dynamics: Climatology (1620); 9305 Information Related to Geographic Region: Africa; *KEYWORDS:* tropical glaciers, Kilimanjaro, ablation, energy balance

Citation: Mölg, T., and D. R. Hardy (2004), Ablation and associated energy balance of a horizontal glacier surface on Kilimanjaro, *J. Geophys. Res.*, *109*, D16104, doi:10.1029/2003JD004338.

1. Introduction and Background

[2] The behavior of glaciers is a manifestation of fluctuations in the climate system. Glaciers thus represent important indicators of climate change, highlighted by the work of *Oerlemans* [2001]. Tropical glaciers are indicators of particular sensitivity, as they are exposed to a climate differing from that of the midlatitudes and high latitudes [*Kaser et al.*, 1996; *Kaser and Osmaston*, 2002]. A pronounced seasonality in tropical climate is exclusively caused by the annual cycle of air humidity and related parameters (e.g., cloudiness, precipitation), while the annual variation of air temperature at all altitudes is small, ensuring the thermal homogeneity of tropical climate in time and space [*Hastenrath*, 1991]. These climatic features exert a complex impact on tropical glacier behavior, making the glaciers especially sensitive to shifts in hygric seasonality [*Kaser*, 2001; *Kaser et al.*, 2004a]. Following the global trend, tropical glaciers have retreated drastically throughout the twentieth century [*Kaser*, 1999; *Georges*, 2004]. The underlying climatic forcing, however, merits further exploration, which was emphasized in the latest report of the *Intergovernmental Panel on Climate Change* [2001] in the context of global warming, since it has not been demonstrated that air temperature is the primary control of tropical glacier recession. The reviews of *Kaser* [1999] and *Kaser et al.* [2004a] suggest instead that changes in air humidity and related climate variables control this recession.

[3] In view of the need to understand glacier-climate interactions in the tropics more completely this study estimates the energy balance (EB) of a horizontal glacier surface on Kilimanjaro, tropical East Africa. The EB of a glacier surface describes the physical connection between climatic forcing and ice/snow ablation and thus provides insight into climatic control of glacier ablation. The Kilimanjaro massif, of volcanic origin, is located ~370 km south of the equator and about the same distance from the Indian Ocean at the Tanzania-Kenya border (3°04′S/37°21′E). Only one of the massif's three peaks is presently

0148-0227/04/2003JD004338$09.00

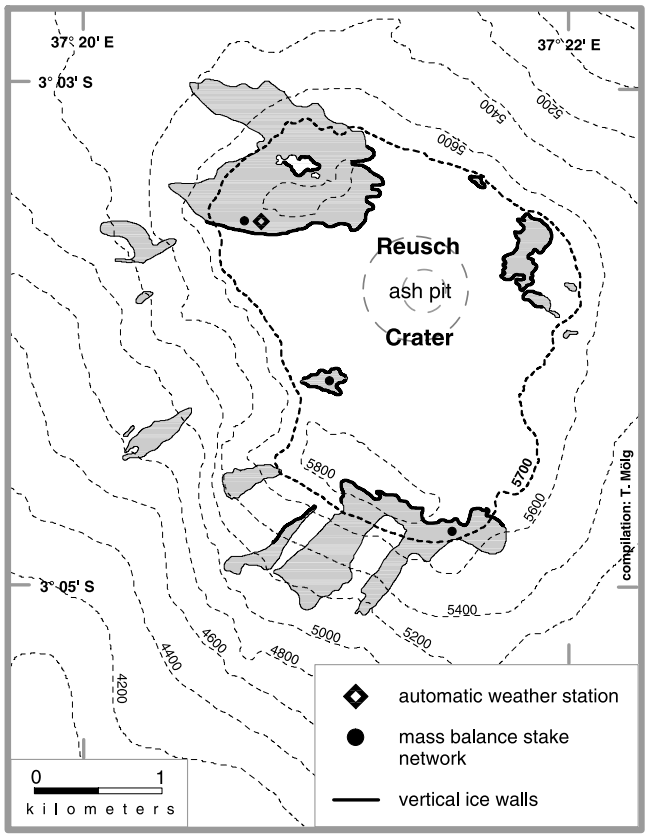

Figure 1. Glacier extent on Kibo in 2000 after *Thompson et al.* [2002], spatial distribution of vertical ice walls (determined stereoscopically from air photographs taken in 2000 and from field experience), and locations of the automatic weather station and mass balance stake networks (map contours in meters and universal time meridian zone 37°S projection). The bold 5700 m contour is a good indicator for delimiting the summit plateau. Map compiled by T. Mölg, October 2002/June 2003.

glacierized, namely, Kibo. Figure 1 depicts Kibo and its glacier extent for the year 2000, based on aerial photographs taken in February of the same year by *Thompson et al.* [2002]. They provide a figure of 2.6 km^2 as the current glacier surface area, greatly reduced from 12 km^2 in 1912 [*Hastenrath and Greischar*, 1997]. The automatic weather station (AWS) providing the main data input for this study is situated on the horizontal surface of the Northern Ice Field (NIF). This is one of Kibo's ice entities on the summit plateau (plateau extent indicated by the 5700 m contour in Figure 1), typically margined by vertical walls and a (near-) horizontal surface (Figure 1). The AWS was installed in February 2000 by University of Massachusetts personnel and has been revisited since then once or twice a year. Mass balance stakes (one since February 2000 (reference stake), four since February 2001, and seven since June 2001) are placed close to the AWS, as shown in Figure 1. Measurement details will follow in section 2.

[4] On a regional scale the background of this study is twofold. First, it has been speculated that general global warming is directly driving the retreat of Kilimanjaro's glaciers [e.g., *Irion*, 2001]. However, detailed analyses of glacier retreat in the global tropics uniformly reveal that changes in climate variables related to air humidity prevail in controlling the modern retreat (e.g., *Kaser and Georges* [1997] for the Peruvian Cordillera Blanca and *Francou et al.* [2003] for the Bolivian Cordillera Real (both South American Andes); *Kruss* [1983], *Kruss and Hastenrath* [1987], and *Hastenrath* [1995] for Mount Kenya (East Africa); and *Mölg et al.* [2003a] for the Rwenzori massif (East Africa)). Second, *Kaser et al.* [2004b] introduced a hypothesis that a strong reduction in precipitation (i.e., reduction in accumulation) at the end of the nineteenth century and associated changes in other climate variables (cloudiness and incoming solar radiation) led to the initiation of modern glacier retreat on Kilimanjaro around 1880 [*Hastenrath*, 1984] and its continuation to the present. This implies a pronounced sensitivity of Kibo's glaciers to precipitation variability, as pointed out by *Hardy* [2003]. The study of *Mölg et al.* [2003b] provides the first detailed support for this hypothesis, showing that solar radiation primarily controls the retreat of the summit vertical ice walls (Figure 1), given the relatively dry East African climate of the twentieth century. Against this background this study on Kibo's surface EB is timely in order to reveal the basic climatic controls of ablation on the summit horizontal glacier surfaces. Also, contrasting ablation between the first 2 years of measurements (see section 2) offers the opportunity to explore which changes in climate parameters induce a strong response of the glacier surface.

[5] The EB characteristics of glacier surfaces in the tropics have been established by the detailed studies of *Wagnon et al.* [1999a, 1999b, 2001, 2003] on the glaciers Zongo and Illimani in the Bolivian Cordillera Real. In East Africa, EB investigations are limited to the efforts of Hastenrath and coworkers, who performed measurements on Lewis Glacier, Mount Kenya, in 1977/1978, which are summarized by *Hastenrath* [1984]. This paper helps to complement the picture of EB characteristics of tropical glaciers, although the AWS on Kibo was initially not designed to drive an energy balance model (see section 2). Nevertheless, the AWS provides a unique multiyear data record from a high-altitude site, which is exceptional for this part of the world and thus justifies the use of parameterizations and assumptions in order to calculate at least robust estimates (i.e., relative magnitudes) of the single EB components. This study's specific aims are (1) to determine on a monthly basis the relative magnitudes of the EB components for the first 2 years of measurements, (2) to detect the climate parameter(s) responsible for the marked difference in ablation between these 2 years, and (3) to provide a qualitative climatological interpretation of the results in the context of modern glacier retreat on Kilimanjaro.

2. Data Basis and Climatic Conditions

2.1. Meteorological Measurements and Climate

[6] The Kibo AWS is located at 5794 m above sea level on the near-horizontal surface of the NIF with a local slope of <1° at least 100 m in all directions. It started operating on 25 February 2000, and the full data set is available until July 2002, the date of the latest field visit at the time of this study. Measurements comprise incoming shortwave radiation relative to a horizontal surface (Eppley 8–48 sensor), aspirated air temperature and relative humidity (Rotronic

MP101A), wind speed and direction (RM Young 05103), surface height change (i.e., accumulation and ablation) measured by two sonic ranging sensors (Campbell Scientific SR50), and barometric air pressure (Setra 270, since June 2001). Wind and radiation measurements are sampled every minute and are then stored as hourly means on a Campbell CR23X data logger, while hourly means of air temperature and humidity result from measurements every 10 min. Surface height change and air pressure are stored as hourly samples. In July 2002 an albedometer (Kipp and Zonen CM 14) was added, providing reflected shortwave radiation data for future studies. Pictures of and further details on the AWS are available on the World Wide Web server for the University of Massachusetts at http://www.geo.umass.edu/climate/kibo.html. The described measurement program precludes a precise determination of absolute values of the EB components, since several of these components must be parameterized (section 3). Nevertheless, it should be possible to reveal the basic characteristics of the EB governing ablation at the glacier surface. This study addresses the first 2 years of measurements, i.e., the time span 1 March 2000 to 28 February 2002. The only data gap in this interval exists between October 2000 and mid-February 2001, since particularly strong ablation in August and September 2000 caused tilting of the station at the beginning of October. This primarily resulted in disturbed measurements of incoming shortwave radiation and surface height change, which are clearly visible in the October data. Thus the EB investigations are limited to the 7 months between March and September 2000 for the first half of the examined time span. These 7 months are henceforth referred to as mass balance period 1 (MBP1), and the second year, 1 March 2001 to 28 February 2002, is referred to as mass balance period 2 (MBP2). Starting the mass balance periods in March is mainly a result of field campaign timing but is also logical in terms of climatic conditions, as clarified in the following paragraph.

[7] Climate in the Kilimanjaro region is characterized by a bimodal distribution of rainfall [*Coutts*, 1969; *Basalirwa et al.*, 1999] due to the seasonal zonal oscillation of the Intertropical Convergence Zone (ITCZ). The so-called "long rains" are centered on March to May, and the so-called "short rains" are centered on October/November to December. Rainy seasons are typically separated by a long and pronounced dry season between June and September and by a shorter dry season in January and February. Hence the mass balance periods as chosen here start with the long rains and, in the case of MBP2, end with the January/February dry season. Mean values of the recorded climate parameters at the AWS for MBP1 and MBP2 are shown in Table 1. An overview of meteorological data including annual and diurnal cycles will be presented in a forthcoming paper. Data in Table 1 reflect the typical climate of a cold and dry high-altitude site in the tropics [e.g., *Hardy et al.*, 1998] with high incoming shortwave radiation amounts, moderate wind speeds, low air humidity, and temperatures clearly below the freezing point. Although East African precipitation seasonality, as explained above, was not well pronounced through 2000 and 2001 [*Waple et al.*, 2002; *Hardy*, 2003], the recorded snowfall and water vapor pressure are the only parameters that experience an obvious annual cycle reflecting rainy and dry seasons, while mean monthly temperatures vary <2°C around the values shown in Table 1 ("thermal homogeneity"). Wind speed seems to undergo a weakly pronounced annual cycle, peaking with the passage of the ITCZ.

Table 1. Mean Values of Incoming Shortwave Radiation, Air Temperature, Air Humidity (Expressed as Water Vapor Pressure), Wind Speed, Barometric Air Pressure, and Monthly Precipitation at the Kibo AWS for Mass Balance Period 1 (MBP1) and Mass Balance Period 2 (MBP2)[a]

Parameter	Height, m	Accuracy	MBP1	MBP2
Incoming shortwave radiation, W m^{-2}	3.4	±3%	313.5	318.6
Air temperature, °C	2.2	±0.3°C	−7.7	−6.8
Water vapor pressure, hPa	2.2	±1%[b]	1.7	2.0
Wind speed, m s^{-1}	3.75	±0.3°m s^{-1}	5.8	5.6
Air pressure,[c] hPa		±<0.05%	NA[d]	505.8
Precipitation/snowfall, cm $month^{-1}$	2.2[e]	±1 cm	10.3	12.2

[a]Values for MBP1 represent a 7 month mean, and those for MBP2 represent a 12 month mean. Air pressure is a mean between 8 June 2001 and 28 February 2002, as explained in the text. Instrument heights refer to the time of installation of the AWS; accuracy refers to manufacturer's information.
[b]Accuracy refers to relative humidity.
[c]Air pressure was measured in electronics enclosure.
[d]NA indicates not available.
[e]Height of sonic ranging sensors is given.

2.2. Analysis of Monthly Ablation

[8] Although there are no marked differences in recorded climate parameters between MBP1 and MBP2 (Table 1), ablation at the AWS differed between these two periods. This appears from the net specific mass balances which were determined on an annual basis between 25 February 2000 and 10 February 2001 (−760 ± 80 mm water equivalent (WE)) and 10 February 2001 and 10 February 2002 (−195 ± 55 mm WE). These contrasting annual balances at the AWS site were reported by *Thompson et al.* [2002] with a slightly different estimate (based on a different surface datum). Annual mass balances are derived from (1) readings of the reference stake during the first two field campaigns (25 February 2000 and 10 February 2001), (2) snow depth recorded by the sonic ranging sensors (SRS) on 10 February 2001 and 10 February 2002 (a continuous record with constant reference surface), and (3) bulk density snowpack measurements in June and August 2001, the latter of which showed values close to 300 kg m^{-3}. The uncertainties given in the parentheses above account for the assumed ice density range (850–900 kg m^{-3}) and the difference in snow depth between the AWS site and the reference stake. Average monthly precipitation (in cm) shown in Table 1, which appears nearly equivalent through the two distinguished periods, as well as anomalously low annual precipitation amounts throughout East Africa in both 2000 and 2001 [*Waple et al.*, 2002] suggest that a difference in ablation, rather than in accumulation, caused the marked difference between the two net specific mass balances. Nevertheless, precipitation (accumulation) and its timing had a decisive impact on the overall EB and thus mass balance by determining the "initial conditions" of MBP1 and MBP2, which will be discussed in connection with the results (section 4).

[9] In order to examine differences in ablation, total specific ablation for each month of MBP1 and MBP2 was

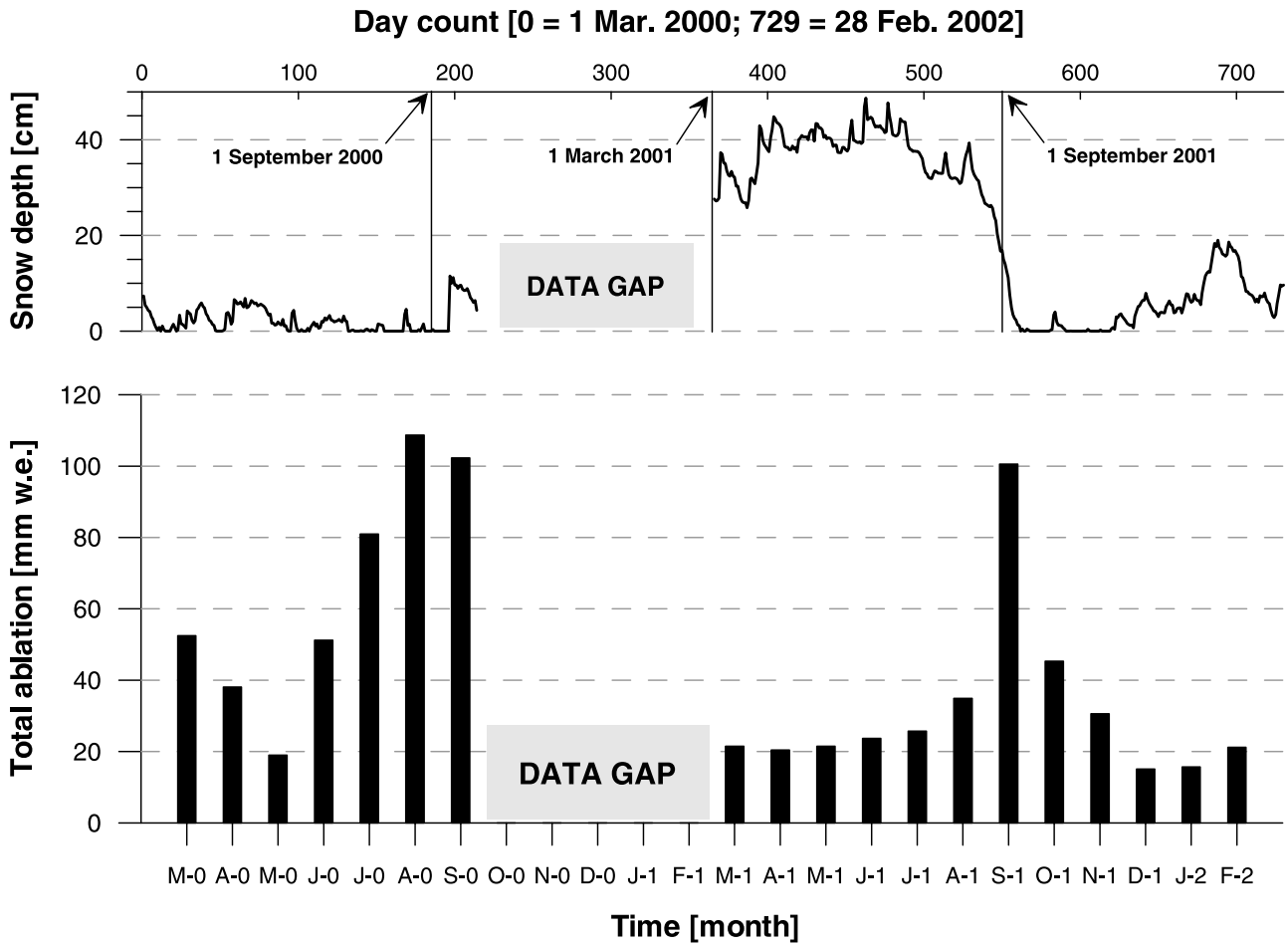

Figure 2. (top) Daily snow depth and (bottom) total monthly ablation between March 2000 and February 2002, as deduced from the sonic ranging sensors data.

deduced from daily SRS data in water equivalents [e.g., *Oerlemans*, 2000; *Hardy et al.*, 2003]. These monthly values also serve to validate the energy balance calculations. The surface condition on 25 February 2000 when the SRS began to operate (glacier ice) as well as on 10 February 2001 when SRS data are again available after reinstalling the tilted AWS (45 cm snow over ice) must, of course, be known. In a preparatory step the period 10 February 2001 to 10 February 2002 was addressed (i.e., the second year of the annual net mass balance determination, without any data gap in the SRS recordings) in order to calibrate a mean snow density, ρ_s. Lowering of the surface with ice exposed was converted to daily water equivalent ablation by an ice density, ρ_i, of 900 kg m^{-3}. Derivation of the mean net balance as measured in this period, −195 mm WE (see above), then requires ρ_s = 145 kg m^{-3} for surface height increase (i.e., accumulation of snow) as well as for surface height lowering with snow exposed (i.e., ablation of snow). Regarding the desired ablation analysis, this calibrated mean value seems close to or a bit higher than the density of fresh snow but lower than the bulk density of older snow as measured (see above). Nevertheless, since density measurements were very limited in time and could have captured special circumstances in the snowpack (e.g., densification by meltwater infiltration), the calibrated value is understood as the relevant mean "long-term" surface density. Water equivalent snow ablation was hence derived by using ρ_s = 145 kg m^{-3} and added to ice ablation (ρ_i = 900 kg m^{-3}).

[10] Figure 2 depicts the resulting cycle of total monthly ablation through MBP1 and MBP2 along with snow depth at the AWS site and clearly demonstrates that mean monthly ablation was higher in MBP1. Continuously high ablation amounts are found between July and September 2000, which ultimately caused tilting of the AWS in October 2000 and resulted in the subsequent data gap. In MBP2, only September 2001 ablation is comparable to those high amounts, which coincides with the vanishing of the seasonal snow cover. Speaking numerically, mean monthly ablation was 2.1 times higher in MBP1 than in MBP2. Despite the uncertainties contained in this determination, which are unavoidable at high-altitude unmanned sites, analysis of the SRS data provides good insight into the temporal variability of ablation on the NIF.

3. Energy Balance Modeling

[11] The energy balance of a glacier surface can be approximated in the following form:

$$R + \mathrm{QS} + \mathrm{QL} + \mathrm{QP} + \mathrm{QG} = F. \quad (1)$$

R symbolizes the energy flux from net radiation (section 3.1), QS and QL symbolize the turbulent sensible heat flux and the turbulent latent heat flux, respectively (section 3.2), QP symbolizes the heat flux supplied by precipitation, and QG symbolizes the total energy flux in the subsurface (section 3.3). The resulting energy flux at the surface is denoted by F. Fluxes toward the surface are defined as positive, and those away from the surface are defined as negative. If the surface temperature is at 0°C and the right-hand side of equation (1) is positive, F represents the latent energy flux for melting, QM. In this study, QP can be neglected since precipitation always falls in a frozen state and precipitation intensities are weak (Table 1). Although the study site is located in a dry and cold climate, where sublimation can represent the only energetic ablation mechanism [e.g., *Bintanja and Van den Broeke*, 1995; *Wagnon et al.*, 2003], melting is considered a possible result of equation (1) in light of the following field observations: (1) rapid accumulation of water in a 1 m deep hole created for the AWS in February 2000, (2) the presence of ice layers in the seasonal snowpack, and (3) evidence for superimposed ice development due to meltwater percolating through the seasonal snow cover and refreezing at the ice interface. Nevertheless, sublimation is expected to dominate the consumption of energy available for ablation and to be a persistent process of mass loss.

3.1. Net Radiation

[12] The energy flux from net radiation, R, is the sum of incoming shortwave radiation, $S\downarrow$, reflected shortwave radiation, $S\uparrow$, incoming longwave radiation, $L\downarrow$, and outgoing longwave radiation, $L\uparrow$. Net radiation is frequently written in the form $R = S\downarrow\ (1 - \alpha) + L\downarrow - L\uparrow$, where α signifies the shortwave albedo of the glacier surface. $S\downarrow$ relative to a horizontal surface is measured directly at the AWS and was not corrected for the tilt of the surface [e.g., *Greuell and Smeets*, 2001] since the local slope at the AWS site is minimal (section 2). The data of $S\uparrow$ are not available yet, and thus α must be parameterized. For that the albedo model of *Oerlemans and Knap* [1998] is used. The advantage of their daily resolution model is that it takes into account the processes determining albedo in more detail than other albedo models do, which is shown by *Klok and Oerlemans* [2004]. The model introduces five control parameters: an albedo of fresh snow not older than 1 day ($\alpha_{frs} = 0.75$), an albedo of firn ($\alpha_{fi} = 0.53$), an albedo of ice ($\alpha_{ice} = 0.34$), an e-folding constant for the effect of aging on snow albedo ($t^* = 21.9$ days), and an e-folding constant for the effect of snow depth on albedo ($d^* = 3.2$ cm). The albedo of the glacier surface at day (i) with snow depth d (in cm) then results from

$$\alpha^{(i)} = \alpha_s^{(i)} + \left(\alpha_{ice} - \alpha_s^{(i)}\right) \exp\left(\frac{-d}{d^*}\right). \quad (2)$$

Within equation (2) the albedo of snow at day (i), $\alpha_s^{(i)}$, is a function of the time since the last snowfall, i.e., the difference between the day number with the last snowfall event, s, and the actual day number, i:

$$\alpha_s^{(i)} = \alpha_{fi} + \left(\alpha_{frs} - \alpha_{fi}\right) \exp\left(\frac{s - i}{t^*}\right). \quad (3)$$

Daily values for d and s are provided by the daily data of the SRS. Only daily accumulation >1 cm was rated as a snowfall event, considering the uncertainty in the SRS measurements [cf. *Hardy et al.*, 2003]. Since the data of the reflected shortwave radiation sensor were not available at the time of this study in order to calibrate the model to Kibo conditions, three of the control parameters are taken from *Oerlemans and Knap* [1998] as given above (α_{fi}, t^*, and d^*). The value for α_{frs} is increased to 0.9 according to the more recent study of *Klok and Oerlemans* [2002]. Ice albedo is also increased ($\alpha_{ice} = 0.45$), since ice surfaces with continuous sublimation, e.g., Antarctic blue ice areas, show an albedo of ~0.45–0.5 in the lowest case [*Bintanja and Reijmer*, 2001].

[13] Many empirical formulas exist to calculate incoming longwave radiation from standard meteorological variables. Most of them rely on a combination of air temperature and air humidity [e.g., *Müller*, 1984] or air temperature, air humidity, and cloudiness [e.g., *Oerlemans*, 2000]. *Duguay* [1993] presented a review of radiation modeling especially in mountainous terrain and suggests the following equation:

$$L\downarrow = \sigma T_a^4 (C_1 + C_2\ e_a). \quad (4)$$

The air temperature at screen level is denoted by T_a (in K), e_a symbolizes the water vapor pressure of the air (in hPa), σ is the Stefan-Boltzmann constant (5.67×10^{-8} W m^{-2} K^{-4}), and C_1 and C_2 are empirical constants (0.554 and 0.017 hPa^{-1}, respectively). To check if these two constants are suitable for high-altitude tropical conditions, equation (4) was tested against 35 days of measured $L\downarrow$ on Illimani, Bolivian Andes, collected over a flat glacier surface during May 2001 and May–June 2002 [*Wagnon et al.*, 2003]. This high-altitude tropical glacier site shows a climatic setting similar to Kibo, with air temperatures always clearly below 0°C, low absolute air humidity, and moderate to high wind speeds. Applied to the mean diurnal cycle of T_a and e_a measurements on Illimani (mean over the 35 days), equation (4) with the constants as given above leads to a mean diurnal underestimation of measured $L\downarrow$ of 31 W m^{-2}. The maximum hourly underestimation even reaches 48 W m^{-2}, which is clearly too much. Hence optimum values for the constants were determined in a correlation analysis, which yielded $C_1 = 0.585$ and $C_2 = 0.062$ hPa^{-1}. The maximum hourly deviation now remains below 15 W m^{-2}, which is acceptable given the general uncertainty of longwave radiation measurements (~10 W m^{-2}). Using these new constants, a better estimate of $L\downarrow$ is also expected for Kibo, since mean vapor pressure conditions on Kibo and Illimani are nearly identical over the respective periods with data coverage (1.87 hPa on Kibo and 1.88 hPa on Illimani). For calculations it is assumed that the longwave radiation field is isotropic within the reach of the AWS, which is reasonable for a glacier surface with a nearly constant slope over 100 m or more [*Oerlemans*, 2000]. Finally, to complete net radiation, $L\uparrow$ is calculated conventionally from the Stefan-Boltzmann law ($L\uparrow = \sigma\ \varepsilon_S T_S^4$) by input of the surface temperature, T_S (in K), as discussed in section 3.3, and the emissivity of the surface,

ε_S. As snow and ice have an emission coefficient close to 1.0 [e.g., *Kuhn*, 1987], ε_S is set to unity.

3.2. Turbulent Heat Exchange

[14] If the turbulent heat fluxes are not measured directly by complex eddy correlation systems [e.g., *Gustafsson et al.*, 2001], they are preferably estimated from methods that are based on the Monin-Obukhov similarity theory [e.g., *Garratt*, 1992]. In this paper, the "bulk method" is used to compute the turbulent heat fluxes by the following analytical expressions (for neutral conditions):

$$\mathrm{QS} = c_p\ \rho_0\ \frac{p}{p_0}\ \frac{k^2 v(T_a - T_S)}{\ln\left(\frac{z_m}{z_{0m}}\right)\ln\left(\frac{z_h}{z_{0h}}\right)} \tag{5}$$

$$\mathrm{QL} = 0.623\ L_V\ \rho_0\ \frac{1}{p_0}\ \frac{k^2 v(e_a - E_S)}{\ln\left(\frac{z_m}{z_{0m}}\right)\ln\left(\frac{z_v}{z_{0v}}\right)}. \tag{6}$$

Air temperature at the measurement height above the surface z_h (in m) is represented by T_a, e_a is the water vapor pressure of the air (in hPa) at the height z_v (in m), and v is wind speed (in m s^{-1}) at height z_m (in m). Surface temperature (section 3.3) and surface vapor pressure (saturation assumed) (in hPa) are symbolized by T_S and E_S, respectively. E_S is typically calculated as a function of T_S. The specific heat of air at constant pressure (1010 J kg^{-1} K^{-1}) is denoted by c_p, ρ_0 is the air density at standard sea level (1.29 kg m^{-3}), p is the actual air pressure (in hPa), p_0 is the air pressure at standard sea level (1013 hPa), k is the von Karman constant (0.4), and L_V is the heat constant for vaporization (2.514 MJ kg^{-1}) which is replaced by the heat constant for sublimation, L_S (2.848 MJ kg^{-1}), if T_S is below the melting point [e.g., *Wagnon et al.*, 2003]. The parameter z_{0m} is the roughness length of momentum (in m) and is a measure of the aerodynamic roughness of the surface. It is defined as the height above the surface where the extrapolated logarithmic profile of wind speed is equal to zero. The scalar roughness lengths of temperature, z_{0h}, and of water vapor, z_{0v}, (both in m) indicate the height above the surface where the logarithmic profile of the respective variable reaches the surface value. Roughness lengths are determined either by profile measurements and the subsequent selection of "near-neutral" profiles [e.g., *Denby and Snellen*, 2002], or alternatively, they are calibrated from sublimation measurements [e.g., *Wagnon et al.*, 2003]. Since such measurements are not yet available from Kibo, a value of 0.1 mm is used for all three roughness lengths, following *Lewis et al.* [1999]. They found this value on the horizontal surface of Canada Glacier (also located in a dry and cold climate, Antarctica) which visually appears to have a roughness element shape quite similar to that of the NIF surface. Still, it must be mentioned that there is both theoretical [e.g., *Andreas*, 1987] and field evidence [e.g., *Greuell and Smeets*, 2001] that $z_{0m} \neq z_{0h} \neq z_{0v}$, the two latter typically being 1–3 magnitudes smaller than z_{0m}. According to the surface renewal theory of *Andreas* [1987] the scalar roughness lengths z_{0h} and z_{0v} can be obtained from z_{0m} and the so-called roughness Reynolds number. This number is a function of the turbulent surface velocity scale (friction velocity), determination of which requires measurement of wind speed at two or more levels. Since wind speed is available at one level only in this case, using similar roughness lengths is supported by (1) several past EB studies showing that it is appropriate to assume similar roughness lengths for smooth glacier surfaces in a dry and cold climate [e.g., *Lewis et al.*, 1999; *Bintanja and Reijmer*, 2001] and (2) a theoretical framework suggesting using similar roughness lengths if the differences between z_{0m} and the scalar roughness lengths are not known [*Sharan et al.*, 2003].

[15] Stability correction is usually considered in terms of the bulk Richardson number (Ri_b) [e.g., *Schneider*, 1999; *Wagnon et al.*, 2003] or the Obukhov length [e.g., *Gustafsson et al.*, 2001]. Here Ri_b is calculated as a function of T_a, T_S, z_m, z_{0m}, v, and the acceleration of gravity (9.81 m s^{-2}) and is inserted into nondimensional stability functions ("Φ functions") which can be applied to equations (5) and (6). *Wagnon et al.* [2003] show this procedure in detail. A note on the stability of the surface boundary layer at the Kibo AWS site is given in section 5.

3.3. Subsurface Energy Flux and Surface Temperature

[16] The total energy flux in the subsurface (QG) consists of an energy flux from penetrating shortwave radiation (QPS) and a conductive heat flux (QC). The former is calculated as a 20% fraction of net shortwave radiation ($S_{\mathrm{net}} = S\downarrow\ (1 - \alpha)$) for days with ice at the surface and as a 10% fraction of S_{net} for days with snow at the surface [*Bintanja and Van den Broeke*, 1995]. Since QPS is directed from the surface into the ground, it always has a negative sign in the EB. Conduction in the subsurface is determined from a simple two-layer soil model as typically used in boundary layer models, which is explained explicitly by *Garratt* [1992]. In this model the temperature of the thin upper layer (of thickness $\Delta z'$) equals the surface temperature (T_S). The deeper soil layer has a constant temperature, T_{DS}, which can be well estimated from temperature profile measurements performed near the AWS in 2000 by *Thompson et al.* [2002]. We use a reference temperature of −1.2°C at a depth of 10 m [*Thompson et al.*, 2002]. The relevant equation then reads $\mathrm{QC} = \mu\ (T_{DS} - T_S)$ [*Garratt*, 1992]. Calculation of μ requires input of the soil-specific thermal diffusivity (k_s), i.e., in this study, k_s for ice or, if daily snow depth exceeds $\Delta z'$, k_s for snow. *Paterson* [1994] lists standard values for these diffusivities.

[17] Surface temperature is solved in an iterative procedure, as done by *Gustafsson et al.* [2001], where T_S converges toward a value such that net radiation equals the sum of turbulent fluxes and the total subsurface energy flux. If the resultant T_S exceeds the melting point, it is reset to 0°C, and the recalculated energy flux on the right-hand side of equation (1) represents latent energy for melting. This approach implies that all the uncertainties contained in the other components (albedo, longwave radiation, roughness, etc.) are "smoothed" by the T_S value. Section 5 will discuss the validity of this approach.

[18] The Kibo AWS site EB is finally computed by the mean diurnal cycle of meteorological variables of each investigated month, with a temporal resolution of 1 hour. A mean diurnal cycle of air pressure (available since June

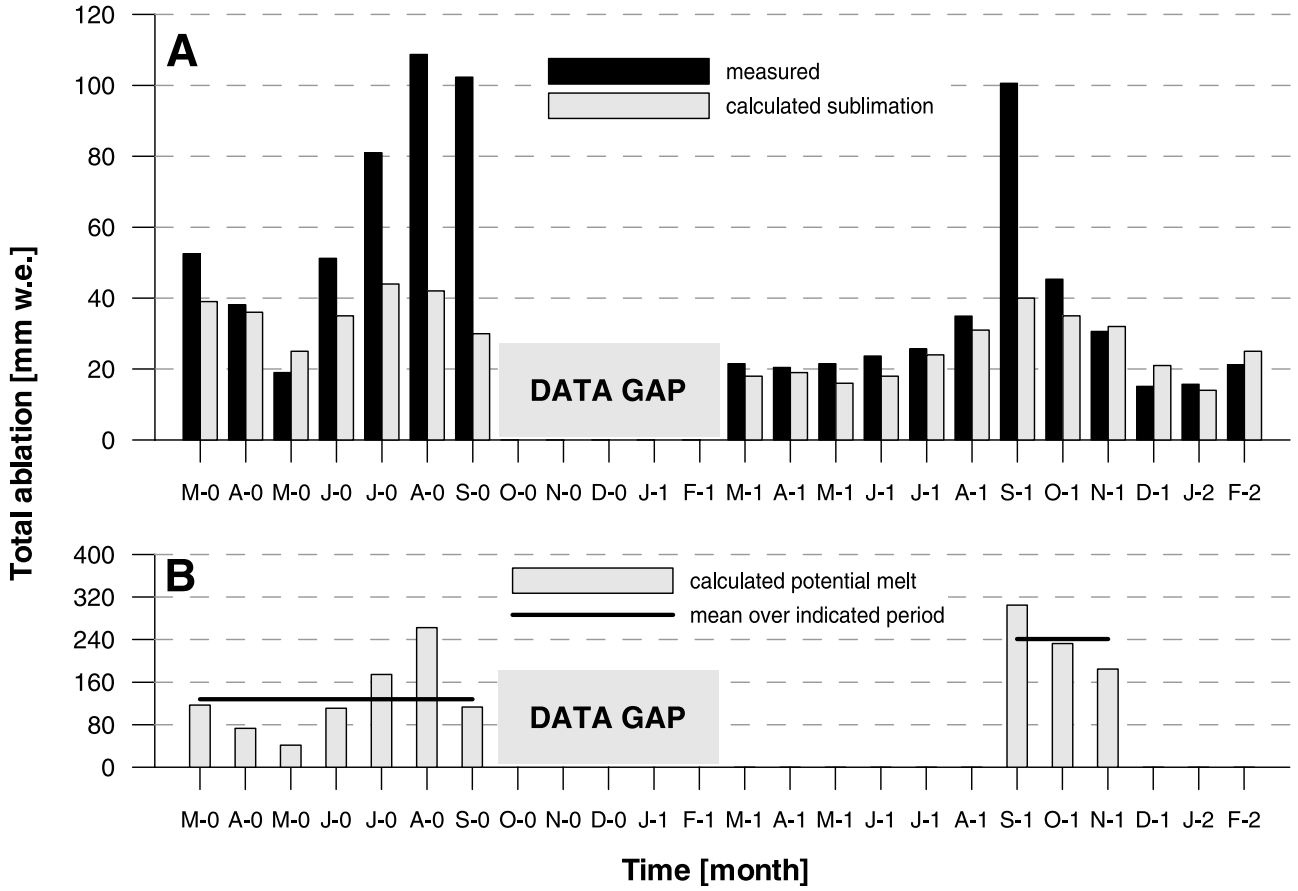

Figure 3. (a) Total monthly ablation as measured in the field and calculated from the turbulent latent heat flux (sublimation) between March 2000 and February 2002 and (b) calculated potential melt over the same period. Note the difference in vertical scales between Figures 3a and 3b.

2001 only) is applied to all months, which is reasonable since (1) the turbulent fluxes' sensitivity to air pressure fluctuations is negligibly small [*Oke*, 1987] and (2) inter-monthly differences in the recorded pressure data are minimal. For each hourly step, specific ablation is calculated from a negative turbulent latent heat flux (QL $\times$ L_S^{-1} for $T_S < 0$°C, QL $\times$ L_V^{-1} for $T_S = 0$°C). Additional ablation by melting is also calculated for periods with a positive surface flux, F, at $T_S = 0$°C from a latent energy flux for melting (QM $\times$ L_M^{-1}), with L_M as the heat constant for fusion (0.334 MJ kg^{-1}). According to the field evidence of meltwater refreezing at the NIF snow-ice interface, or within the snowpack, it can be expected that calculated sublimation largely accounts for the observed ablation. Melting can appear as measured ablation only if the melted water represents mass loss from the site (i.e., runoff).

4. Results

[19] Figure 3a presents a validation of the EB calculations by comparing modeled sublimation with measured ablation as described in section 2. Because of the uncertainties involved in the determination of both quantities one should first concentrate on the comparison of simulated and measured trends rather than on differences in absolute values. This view indicates that both cycles show the same trends, i.e., the development around the MBP1 minimum in May 2000 and the MBP2 broad peak in September 2001. Still, from July to September 2000 and in September 2001, large differences between calculated sublimation and measured ablation are apparent, suggesting that melting occurs during these periods and contributes to ablation. To pursue this conjecture, Figure 3b depicts the cycle of calculated potential melt, i.e., the glacier mass that could be removed, on the basis of the available latent energy flux for melting, if all the melted mass ran off. In a first assessment it seems that energetic conditions for melt must be above average over a coherent period to induce ablation by meltwater, whereas only a fraction of potential melt is converted into actual mass loss (compare y axis scales of Figures 3a and 3b). This is true for July and August 2000 and for September 2001 and conforms to *Kaser et al.*'s [2004b] observation of any runoff intervals on the Kibo plateau being brief and insignificant. However, September 2000 melt conditions obviously do not follow this rule, so this assessment remains a bit speculative. Nonetheless, the combined view of Figures 3a and 3b strengthens the field evidence interpretation that melting does take place at the surface but, at the flat AWS site at least, does not cause substantial ablation because of refreezing of meltwater within the snowpack, at the ice surface, or within the ice body. The latter is indicated by melt features in the NIF ice

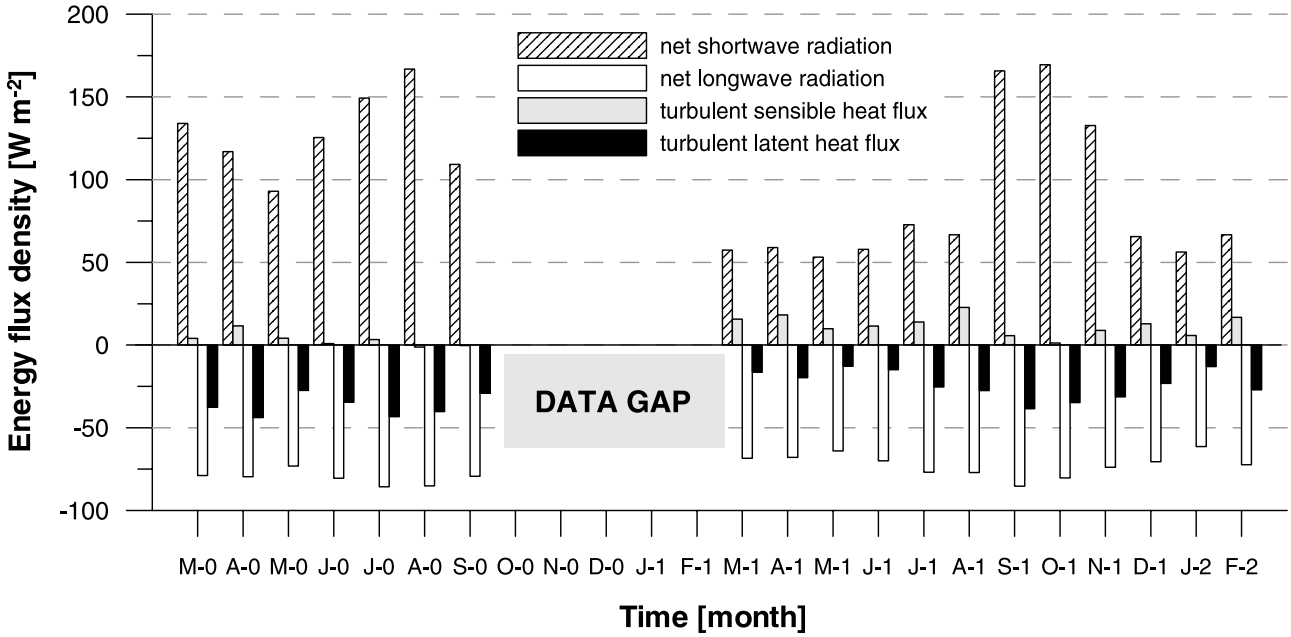

Figure 4. Temporal distribution of the atmospheric energy balance components between March 2000 and February 2002. Net radiation is split into net shortwave and net longwave radiation. Energy flux densities represent the mean value for each month.

cores [*Thompson et al.*, 2002]. The particular circumstances determining the extent that melted water actually contributes to surface ablation need to be better quantified in the future. However, calculated sublimation agrees well with measured ablation in months without potential melt (March to August 2001 and December 2001 to February 2002) or with clear below-average potential melt (e.g., April and May 2000 and November 2001) (Figure 3), and this instills confidence in the computed EB. The pattern of calculated sublimation underestimating measured ablation between March and August 2001, when no latent energy for melting is available (Figure 3b), could point to mechanical ablation by wind scour, as these are the only months in either period with a persistent snowpack at least 20 cm deep (see Figure 2).

[20] The temporal distribution of the atmospheric EB components on the NIF is depicted by Figure 4 on a monthly basis. Net radiation, R, is split into net shortwave radiation ($S_{net} = S\downarrow\ (1 - \alpha)$) and net longwave radiation ($L_{net} = L\downarrow - L\uparrow$). Clearly, radiative exchange dominates the EB throughout the examined periods. Since L_{net} only varies moderately over the months, R is governed by the marked variations in S_{net}. The turbulent latent heat flux, QL, is the second important energy flux and is always negative, indicating strong sublimation. The mean sublimation rate amounts to 0.92 mm WE d^{-1}, comparable to those on other tropical glaciers [e.g., *Wagnon et al.*, 1999b, 2003]. Since East African precipitation seasonality was disrupted in the investigated period [*Waple et al.*, 2002; *Hardy*, 2003], the annual cycle with a more negative QL in the typical dry seasons and a less negative QL in the typical rainy seasons [*Wagnon et al.*, 1999a, 2001] is not pronounced. The turbulent sensible heat flux, QS, is small but a source of energy at the glacier surface. Table 2 summarizes the results, with mean values of the single EB components and associated parameters for MBP1 and MBP2. Table 2 confirms what Figure 4 depicts: The main difference in the EB between the two years is shown by the S_{net} term, which affects R to nearly the same extent. Since incoming shortwave radiation, $S\downarrow$, differed negligibly (Table 1) compared to the difference in S_{net} (Table 2), the strongly different albedo ($\Delta\alpha = -0.15$ in MBP1) must be regarded as controlling this marked interperiodical variation in the EB. To further illustrate this important result, Figure 5 shows the daily albedo for MBP1 and MBP2, as simulated with the albedo model explained in section 3.1. Two associated

Table 2. Mean Values of the Single Energy Balance Components and Associated Parameters at the Kibo AWS Site for MBP1 and MBP2[a]

Component or Parameter	MBP1	MBP2	MBP1 Minus MBP2
Measured ablation, mm WE $month^{-1}$	65	31	34
Net shortwave radiation, W m^{-2}	127.8	85.2	42.6
Albedo	0.59	0.74	−0.15
Net longwave radiation, W m^{-2}	−80.3	−72.3	−8
Net radiation, W m^{-2}	47.5	12.9	34.6
Turbulent latent heat flux, W m^{-2}	−36.5	−23.7	−12.8
Turbulent sensible heat flux, W m^{-2}	3.2	12.0	−8.8
Total subsurface energy flux, W m^{-2}	1.8	6.3	−4.5
Latent energy flux for melting, W m^{-2}	−16.0	−7.5	−8.5
Energy for ablation consumed by sublimation, %	72[b]	86[b]	−14
Snowfall frequency, events $month^{-1}$	2.4	4.2	−1.8

[a]Values represent a 7 month mean for MBP1 and a 12 month mean for MBP2.

[b]Only negative hourly values of the latent heat flux (QL) represent energy available for ablation. Since QL is sometimes positive during the night hours (frost deposition), mean QL/(QL+ QM) as they are shown in Table 2 result in slightly lower percentage values (QM is the latent energy flux for melting).

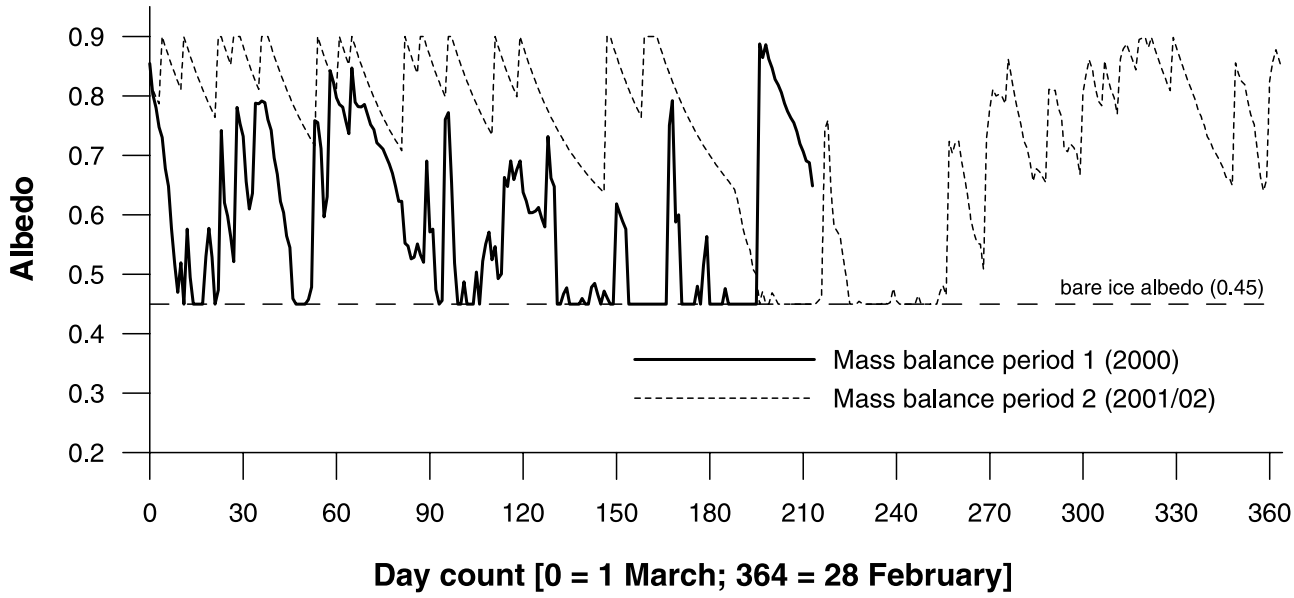

Figure 5. Comparison of daily albedo as derived from the albedo model (section 3.1) between mass balance period 1 and mass balance period 2. Note that mass balance period 1 ends on 30 September (day 213) because of the subsequent data gap (until February 2001). The horizontal dashed line depicts bare ice albedo, defined as 0.45 in the model.

circumstances account for the difference in albedo between the two periods. First, ~50% of the precipitation amount between March 2000 and February 2001 was centered at the anomalous January 2001, a month with extreme precipitation in East Africa [*Waple et al.*, 2002]. Thus considerable snow blanketed the glacier at the beginning of MBP2, protecting the ice surface (see Figure 2). Only in mid-September 2001, ice was exposed again at the surface (approximately day 565 in Figure 2), leading to strong ablation. Second, although absolute precipitation amounts in the Kilimanjaro region between the first and second half of the March 2000 to February 2002 period hardly differed [*Waple et al.*, 2002], the higher snowfall frequency in MBP2 (Table 2) helped to maintain a continuously higher albedo. To conclude, the higher albedo in MBP2 decisively reduced S_{net}, which decreased the latent turbulent heat flux as well as the latent energy flux for melting. Hence the variation in albedo between MBP1 and MBP2 represents the key mechanism explaining the differing ablation. Regarding the partition of ablation energy, sublimation dominates the consumption of energy available for ablation (Table 2). The total subsurface energy flux may be negligibly small on a monthly and longer-term view (Table 2), but it exerts an important diurnal effect (surface heating during the night and cooling during the day) if surface temperature is determined as the unknown variable in the EB.

5. Discussion

[21] Section 4 began the discussion of results specifically pertaining to the NIF. This section focuses on (1) the broader relevance of the results in view of the general EB characteristics of tropical glaciers (section 5.1), (2) the reliability of the methodical approach and the impact of input uncertainties on the overall findings (section 5.2), and (3) how the results obtained for the NIF can be placed in the longer context of modern glacier retreat on Kibo (section 5.3).

5.1. Energy Balance Characteristics of Tropical Glaciers

[22] The results presented in section 4 meet the typical features of the EB on tropical glacier surfaces with potential melting, as established by *Hastenrath* [1984] for Lewis Glacier (Mount Kenya) and *Wagnon et al.* [1999a, 1999b, 2001] for Zongo Glacier (Bolivian Andes). The main energy exchange at the glacier-atmosphere interface results from the terms accounting for net radiation, governed by the variation in net shortwave radiation. The surface albedo, in turn, directly controls net shortwave radiation receipt. Therefore a particular sensitivity of tropical glaciers to albedo, and thus precipitation variability, is a logical consequence, which has been found earlier for Bolivian glaciers on interannual [*Wagnon et al.*, 2001] and decadal timescales [*Francou et al.*, 2003]. The turbulent latent heat flux emerges as the second important energy flux in the tropical glacier EB and is negative all year round, resulting in continuous sublimation. Turbulent exchange of sensible heat remains considerably smaller and of little importance but is usually a minor heat gain.

5.2. Methodical Approach and Input Uncertainties

[23] Do the methodical approach and/or the uncertainties in input parameters as modeled or assumed in order to compute the EB affect the clear order of relative magnitudes of the EB components? The central variable in the methodical approach used here is surface temperature (T_S), as it closes the EB and directly determines outgoing longwave radiation ($L\uparrow$), the turbulent heat fluxes (QL and QS), and the conductive heat flux (see section 3). Although this study is basically directed to monthly and multimonthly characteristics of the EB, Figure 6 offers a look at the mean diurnal

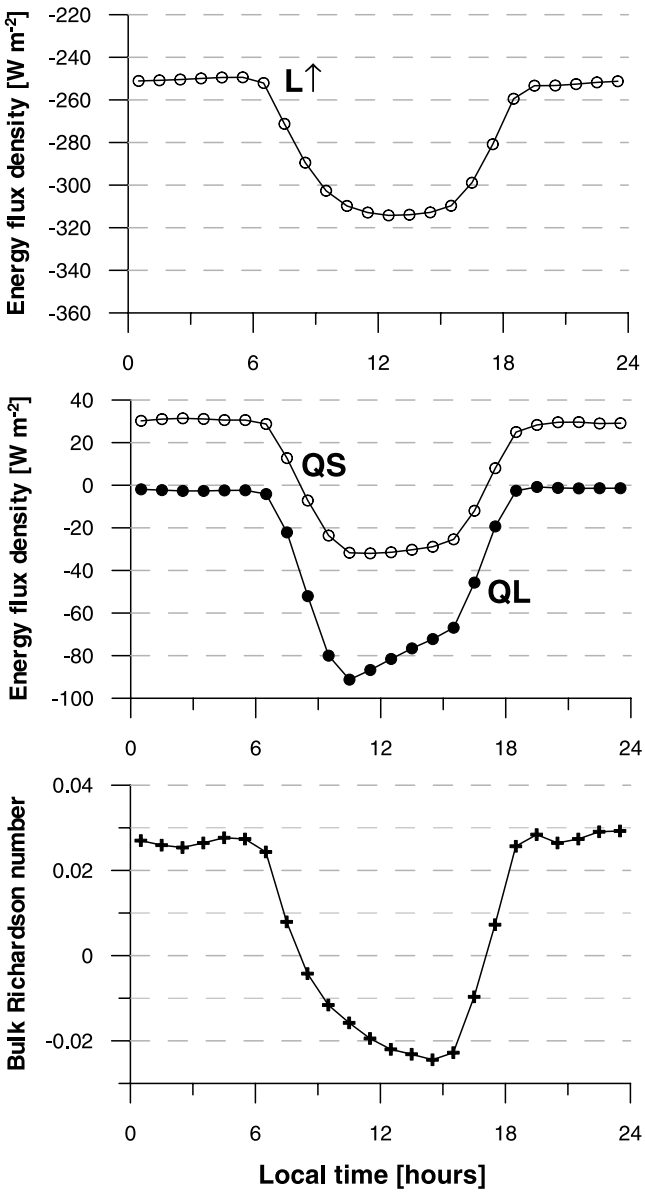

Figure 6. Mean diurnal cycles (based on the 19 investigated months) of (top) outgoing longwave radiation, (middle) turbulent sensible heat flux (QS) and turbulent latent heat flux (QL), and (bottom) bulk Richardson number.

cycles of $L\uparrow$, QL and QS, and Ri_b. These cycles compare very well with those reported from similar climate zones, e.g., from the high-altitude glacier on Illimani [*Wagnon et al.*, 2003] and from inland Antarctica [*Bintanja and Van den Broeke*, 1995]. $L\uparrow$ is nearly constant through the night hours and peaks shortly after midday. QS strongly heats the surface at nighttime stable conditions (Ri_b positive) and changes to negative values during daytime unstable conditions (Ri_b negative). The somewhat greater amplitude of Ri_b on Kibo than on Illimani (not shown) seems realistic, as wind speed on Illimani is much higher, which favors a development toward neutral conditions. QL is close to zero during the night but indicates a considerable heat loss during the day. Since the EB calculations of *Wagnon et al.* [2003] and *Bintanja and Van den Broeke* [1995] are based on more extensive atmospheric measurements than on Kibo, good agreement supports the methodical approach here in addition to the satisfactory validation in section 4.

[24] This leaves, of course, the question of how the uncertainties due to parameterizations and assumptions impact the main results. Figure 7 addresses this issue, showing the relative magnitudes of the EB components in four different cases (model runs). Case 1 represents the initial run as shown in section 4 and Table 2. The uncertainties in the radiation terms are addressed by case 2. For that, albedo is increased by 0.1, which is much higher than the root-mean-square distance in the original model [*Oerlemans and Knap*, 1998], while keeping 0.9 as the accepted upper limit [*Wagnon et al.*, 2003]. A decrease in albedo is not a useful test, as this would strengthen the importance of the radiation terms even more (see MBP1 minus MBP2 in Table 2). Incoming longwave radiation is also changed by an offset 1.5 times the hourly deviation "measured minus modeled" $L\downarrow$ on Illimani. Results show that S_{net} loses relative importance, which is compensated by increases in QS and QG, while L_{net} gains importance. Case 3 addresses the turbulent heat fluxes. Generally, the "bulk method" used here is more accurate than the "profile method," the second method based on the Monin-Obhukov similarity theory, for two reasons. First, the bulk method yields better results even over glacier surfaces with a near-surface katabatic wind speed maximum [*Denby and Greuell*, 2000], which is not related to conditions on the flat and gradient wind-exposed NIF surface. Second, it shows better agreement with eddy correlation measure-

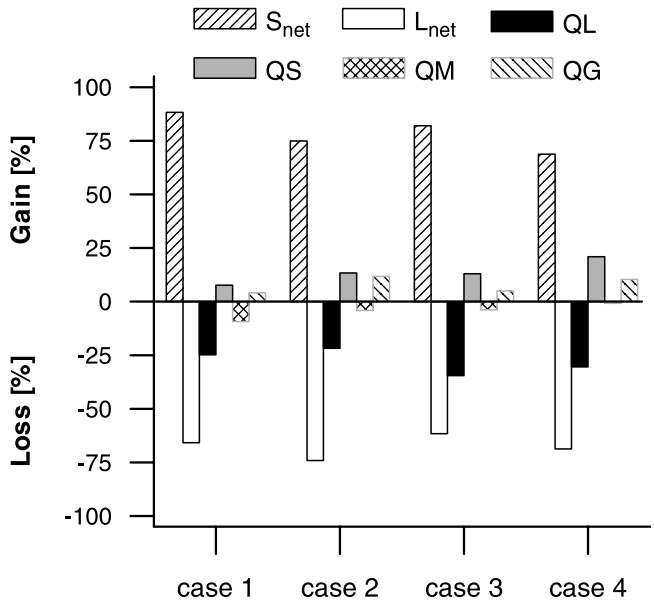

Figure 7. Relative magnitudes of the energy balance components in four different cases (means over the 19 investigated months). Case 1 represents the initial run (Table 2). The energy balance model was also run with offsets in albedo and incoming longwave radiation (case 2) and with increased aerodynamic roughness lengths (case 3), while case 4 combines cases 2 and 3. Details are provided in section 5.

ments, particularly in air temperatures below 0°C [*Arck and Scherer*, 2002], and this second reason is indeed relevant to the conditions on Kibo. Nevertheless, the bulk method is not only especially sensitive to surface temperature (as discussed above) but also to the surface roughness lengths [e.g., *Hock and Holmgren*, 1996]. Hence the EB model was run with roughness lengths 1 order of magnitude greater ($z_{0m} = z_{0h} = z_{0v} = 1$ mm) than the initial case. This results in an increased turbulent heat exchange, compared to case 1. Case 4 combines the offsets of cases 2 and 3, and turbulent heat exchange again gains importance relative to case 1. Despite all the uncertainties, Figure 7 confirms the order of relative magnitudes in the EB: radiation terms (largest), turbulent latent heat flux (intermediate), and turbulent sensible heat flux (smaller). Since uncertainties in measurements (Table 1) are small compared to those from parameterizations and assumptions, they do not influence this main finding.

5.3. Energy Balance in Light of Glacier Retreat

[25] To finally fulfill the third aim of this paper as defined in section 1, how can the EB results be integrated in the context of modern glacier recession on Kilimanjaro? The results of this study confirm the extreme sensitivity of Kibo's horizontal glacier surfaces to precipitation variability which governs the variations in albedo, as mentioned by *Hardy* [2003]. This finding supports present knowledge of climatic forcing of modern glacier retreat on Kilimanjaro, wherein a strong reduction in precipitation at the end of the nineteenth century is regarded as the main reason for the retreat [*Hastenrath*, 1984, 2001; *Kaser et al.*, 2004b]. The ensuing accumulation deficit induced by drier conditions enhanced the ablation term in the glacier mass balance considerably, which was demonstrated for the summit vertical ice walls by *Mölg et al.* [2003b]. Further, the results of this study help clarify the differential ablation between the summit horizontal ice surfaces (moderate lowering) and the summit vertical ice walls (strong lateral retreat) during the twentieth century [*Kaser et al.*, 2004b]. As shown, sublimation dominates the energy consumption on horizontal surfaces, while vertical ice wall ablation is mainly determined by solar radiation-controlled melting [*Mölg et al.*, 2003b] which is ~8 times more effective than sublimation at ablating ice ($L_S \times L_M^{-1} = 8.53$). For the decades prior to 1880, when East African glaciers maintained their latest maximum extent [*Hastenrath*, 2001], *Kruss* [1983] estimated 150 mm yr^{-1} additional precipitation (~15–20% of present precipitation), together with a higher albedo, from a numerical glacier model of Lewis Glacier, located on nearby Mount Kenya. Assuming an albedo on the NIF surface even higher than in this study's MBP2, which would decrease ablation further, and higher precipitation amounts [*Kruss*, 1983], which would increase accumulation, a neutral or positive mass balance could be possible. However, this possibility will remain a qualitative assessment until the Kibo measurement program is expanded in order to calculate the EB on horizontal glacier surfaces more precisely.

[26] Nonetheless, the earlier statement in this section regarding the glacier's extreme sensitivity to precipitation variability can be illustrated by a sensitivity analysis as shown in Table 3. Moderate offsets in air temperature (T_a) clearly induce fewer changes in potential specific ablation than moderate offsets in precipitation (P) ("potential" refers to the fact that it is not yet clear how much melting contributes to actual ablation, see section 4). The 20% precipitation changes are chosen in accordance with *Kruss* [1983] and in the model were only expressed as change in the amount (P frequency and seasonal distribution constant). Changes in accumulation are also listed in Table 3 to once again highlight that P changes affect both glacier mass balance terms and that both terms govern the mass balance signal in the same direction. Any realistic changes in T_a on Kibo will only affect the ablation term, as the plateau glaciers are located far above the mean freezing level (see Table 1) which determines the phase of P (snow or liquid water). This sensitivity analysis clarifies the peculiar nature of Kibo's plateau glaciers and clearly distinguishes them from midlatitude and high-latitude glaciers which are usually more sensitive to T_a changes than to P changes [e.g., *Klok and Oerlemans*, 2002]. It also distinguishes them, though to a lesser extent, from other tropical glaciers which are located at lower elevations near freezing level. There changes in T_a can become more effective than on Kibo, e.g., on the glaciers Lewis [*Hastenrath and Kruss*, 1992] and Zongo [*Wagnon et al.*, 2001].

Table 3. Sensitivity of Potential Specific Ablation (a) to Changes in Air Temperature (T_a) and Precipitation (P)[a]

Forcing	Δa, mm WE month^{-1}	Δc, mm WE month^{-1}
$\Delta T_a = -1$°C	−14.2	0
$\Delta P = +20\%$	−72.1	+4.2
$\Delta T_a = +1$°C	+19.5	0
$\Delta P = -20\%$	+63.8	−4.2

[a]Values are mean monthly sums based on the 19 investigated months. Present-day accumulation at the AWS site is considered to be ~250 mm WE yr^{-1} [*Hardy*, 2003], so given P changes contribute ~4.2 mm WE month^{-1} (= 0.2 × 250/12) to changes in specific accumulation (c).

6. Conclusions

[27] Toward understanding Kilimanjaro's glacier response to climatic forcing more completely, this study revealed the basic characteristics of the EB on a horizontal glacier surface at the summit from data recorded by an AWS. The EB is dominated by radiative exchange which is governed by the variation in net shortwave radiation. The turbulent latent heat flux follows as the second most intensive energy flux. It is negative throughout the year, denoting continuous sublimation. The turbulent sensible heat flux remains small, which indicates the marginal role of local air temperature by itself on ablation. The reason for the striking difference in ablation between the examined mass balance periods (2000 and 2001/2002) is contrasting net shortwave radiation. This component, in turn, is determined by the shortwave surface albedo which differed markedly between the periods. A higher snowfall frequency, together with a thicker snow layer protecting the glacier surface, helped to maintain a continuously higher albedo in the second period. This higher surface reflectivity reduced net shortwave radiation, providing less energy for both energetic ablation processes (sublimation and melting). Melting does occur at the surface but appears to have a temporally varying efficiency for ablation because of refreezing of meltwater within the glacier body. However, sublimation represents the dominant ablation process, con-

suming the majority of energy available for ablation. For future EB studies on the NIF it would be desirable to compare calculated sublimation to direct sublimation measurements, providing a more robust validation.

[28] Placing the results in the context of modern glacier retreat on Kilimanjaro, a particular sensitivity of the summit horizontal glacier surfaces to precipitation variability (magnitude and timing) can be confirmed by this study. This fits well into the present knowledge of modern glacier retreat on Kilimanjaro and in East Africa in general, initiated by a drastic reduction in precipitation at the end of the nineteenth century [*Hastenrath*, 1984, 2001; *Kaser et al.*, 2004b]. Subsequent shifts in the glacier mass balance (reduced accumulation and increased ablation in a relative and an absolute sense) maintained the retreat until the present [*Mölg et al.*, 2003b]. Several studies on glacier behavior in the global tropics have demonstrated the extreme sensitivity of these glaciers to variations in air humidity and related variables like precipitation, surface albedo, cloudiness, and incoming shortwave radiation [e.g., *Kruss*, 1983; *Kruss and Hastenrath*, 1987; *Kaser and Georges*, 1997; *Wagnon et al.*, 1999b, 2001; *Francou et al.*, 2003; *Mölg et al.*, 2003a]. This sensitivity induces especially strong responses from tropical glaciers, presently recession, to climate variability including changes in moisture.

[29] **Acknowledgments.** This material is based upon work supported by the U.S. National Science Foundation under grant 9909201 (University of Massachusetts) and by the Austrian Science Foundation (FWF) under grant P17415-N10 (University of Innsbruck). Special thanks to Patrick Wagnon and his team (LGG, IRD) for providing the Illimani data and to Georg Kaser, Friedrich Obleitner, Michael Kuhn, and Lisette Klok for helpful advice. The detailed comments of three anonymous reviewers helped to improve this study.

References

Andreas, E. L. (1987), A theory for scalar roughness and the scalar transfer coefficient over snow and sea ice, *Boundary Layer Meteorol.*, *38*, 159–184.

Arck, M., and D. Scherer (2002), Problems in the determination of sensible heat flux over snow, *Geogr. Ann.*, *84A*, 157–169.

Basalirwa, C. P. K., J. O. Odiyo, R. J. Mingodo, and E. J. Mpeta (1999), The climatological regions of Tanzania based on the rainfall characteristics, *Int. J. Climatol.*, *19*, 69–80.

Bintanja, R., and C. H. Reijmer (2001), Meteorological conditions over Antarctic blue-ice areas and their influence on the local surface mass balance, *J. Glaciol.*, *47*, 37–50.

Bintanja, R., and M. Van den Broeke (1995), The surface energy balance of Antarctic snow and blue ice, *J. Appl. Meteorol.*, *34*, 902–926.

Coutts, H. H. (1969), Rainfall of the Kilimanjaro area, *Weather*, *24*, 66–69.

Denby, B., and W. Greuell (2000), The use of bulk and profile methods for determining surface heat fluxes in the presence of glacier winds, *J. Glaciol.*, *46*, 445–452.

Denby, B., and H. Snellen (2002), A comparison of surface renewal theory with the observed roughness length for temperature on a melting glacier surface, *Boundary Layer Meteorol.*, *103*, 459–468.

Duguay, C. R. (1993), Radiation modelling in mountainous terrain: Review and status, *Mt. Res. Dev.*, *13*, 339–357.

Francou, B., M. Vuille, P. Wagnon, J. Mendoza, and J.-E. Sicart (2003), Tropical climate change recorded by a glacier in the central Andes during the last decades of the twentieth century: Chacaltaya, Bolivia, 16°S, *J. Geophys. Res.*, *108*(D5), 4059, doi:10.1029/2002JD002473.

Garratt, J. R. (1992), *The Atmospheric Boundary Layer*, Cambridge Univ. Press, New York.

Georges, C. (2004), The 20th century glacier fluctuations in the Cordillera Blanca (Perú), *Arct. Antarct. Alp. Res.*, in press.

Greuell, W., and P. Smeets (2001), Variations with elevation in the surface energy balance on the Pasterze (Austria), *J. Geophys. Res.*, *106*(D23), 31,717–31,727.

Gustafsson, D., M. Stähli, and P. E. Jansson (2001), The surface energy balance of a snow cover: Comparing measurements to two different model simulations, *Theor. Appl. Climatol.*, *70*, 81–96.

Hardy, D. R. (2003), Kilimanjaro snow, *Bull. Am. Meteorol. Soc.*, *84*, S1–S68.

Hardy, D. R., M. Vuille, C. Braun, F. Keimig, and R. S. Bradley (1998), Annual and daily meteorological cycles at high altitude on a tropical mountain, *Bull. Am. Meteorol. Soc.*, *79*, 1899–1913.

Hardy, D. R., M. Vuille, and R. S. Bradley (2003), Variability of snow accumulation and isotopic composition on Nevado Sajama, Bolivia, *J. Geophys. Res.*, *108*(D22), 4693, doi:10.1029/2003JD003623.

Hastenrath, S. (1984), *The Glaciers of Equatorial East Africa*, D. Reidel, Norwell, Mass.

Hastenrath, S. (1991), *Climate Dynamics of the Tropics*, Kluwer Acad., Norwell, Mass.

Hastenrath, S. (1995), Glacier recession on Mount Kenya in the context of the global tropics, *Bull. Inst. Fr. Etud. Andines*, *24*, 633–638.

Hastenrath, S. (2001), Variations of East African climate during the past two centuries, *Clim. Change*, *50*, 209–217.

Hastenrath, S., and L. Greischar (1997), Glacier recession on Kilimanjaro, East Africa, 1912–89, *J. Glaciol.*, *43*, 455–459.

Hastenrath, S., and P. D. Kruss (1992), The dramatic retreat of Mount Kenya's glaciers between 1963 and 1987: Greenhouse forcing, *Ann. Glaciol.*, *16*, 127–133.

Hock, R., and B. Holmgren (1996), Some aspects of energy balance and ablation of Storglaciären, northern Sweden, *Geogr. Ann.*, *78A*, 121–131.

Intergovernmental Panel on Climate Change (2001), *Climate Change 2001: The Scientific Basis*, edited by J. T. Houghton et al., Cambridge Univ. Press, New York.

Irion, R. (2001), The melting snows of Kilimanjaro, *Science*, *291*, 1690–1691.

Kaser, G. (1999), A review of the modern fluctuations of tropical glaciers, *Global Planet. Change*, *22*, 93–103.

Kaser, G. (2001), Glacier-climate interaction at low latitudes, *J. Glaciol.*, *47*, 195–204.

Kaser, G., and C. Georges (1997), Changes in the equilibrium line altitude in the tropical Cordillera Blanca (Perú) between 1930 and 1950 and their spatial variations, *Ann. Glaciol.*, *24*, 344–349.

Kaser, G., and H. Osmaston (2002), *Tropical Glaciers*, Cambridge Univ. Press, New York.

Kaser, G., S. Hastenrath, and A. Ames (1996), Mass balance profiles on tropical glaciers, *Z. Gletscherkd. Glazialgeol.*, *32*, 75–81.

Kaser, G., C. Georges, I. Juen, and T. Mölg (2004a), Low-latitude glaciers: Unique global climate indicators and essential contributors to regional fresh water supply: A conceptual approach, in *Global Change and Mountain Regions: A State of Knowledge Overview*, edited by U. Huber, H. K. M. Bugmann, and M. A. Reasoner, Kluwer Acad., Norwell, Mass., in press.

Kaser, G., D. R. Hardy, T. Mölg, R. S. Bradley, and T. M. Hyera (2004b), Modern glacier retreat on Kilimanjaro as evidence of climate change: Observations and facts, *Int. J. Climatol.*, *24*, 329–339.

Klok, E. J., and J. Oerlemans (2002), Model study of the spatial distribution of the energy and mass balance of Morteratschgletscher, Switzerland, *J. Glaciol.*, *48*, 505–518.

Klok, E. J., and J. Oerlemans (2004), Modelled climate sensitivity of the mass balance of Morteratschgletscher and its dependence on albedo parameterization, *Int. J. Climatol.*, *24*, 231–245.

Kruss, P. D. (1983), Climate change in East Africa: A numerical simulation from the 100 years of terminus record at Lewis Glacier, Mount Kenya, *Z. Gletscherkd. Glazialgeol.*, *19*, 43–60.

Kruss, P. D., and S. Hastenrath (1987), The role of radiation geometry in the climate response of Mount Kenya's glaciers, part 1: Horizontal reference surfaces, *Int. J. Climatol.*, *7*, 493–505.

Kuhn, M. (1987), Micro-meteorological conditions for snow melt, *J. Glaciol.*, *33*, 24–26.

Lewis, K. J., A. G. Fountain, and G. L. Dana (1999), How important is cliff melt?: A study of the Canada Glacier terminus, Taylor Valley, Antarctica, *Global Planet. Change*, *22*, 105–115.

Mölg, T., C. Georges, and G. Kaser (2003a), The contribution of increased incoming shortwave radiation to the retreat of the Rwenzori Glaciers, East Africa, during the 20th century, *Int. J. Climatol.*, *23*, 291–303.

Mölg, T., D. R. Hardy, and G. Kaser (2003b), Solar-radiation-maintained glacier recession on Kilimanjaro drawn from combined ice-radiation geometry modeling, *J. Geophys. Res.*, *108*(D23), 4731, doi:10.1029/2003JD003546.

Müller, H. (1984), *Zum Strahlungshaushalt in den Alpen*, Versuchsanst. für Wasserbau, Hydrol. und Glaziol., Zürich, Switz.

Oerlemans, J. (2000), Analysis of a 3 year meteorological record from the ablation zone of Morteratschgletscher, Switzerland: Energy and mass balance, *J. Glaciol.*, *46*, 571–579.

Oerlemans, J. (2001), *Glaciers and Climate Change*, A. A. Balkema, Brookfield, Vt.

Oerlemans, J., and W. H. Knap (1998), A 1 year record of global radiation and albedo in the ablation zone of Morteratschgletscher, Switzerland, *J. Glaciol.*, *44*, 231–238.

Oke, T. R. (1987), *Boundary Layer Climates*, Methuen, New York.

Paterson, W. S. B. (1994), *The Physics of Glaciers*, 3rd ed., Oxford Univ. Press, New York.

Schneider, C. (1999), Energy balance estimates during the summer season of glaciers of the Antarctic Peninsula, *Global Planet. Change*, *22*, 117–130.

Sharan, M., T. V. B. P. S. Rama Krishna, and Aditi (2003), Surface-layer characteristics in the stable boundary layer with strong and weak winds, *Boundary Layer Meteorol.*, *108*, 257–288.

Thompson, L. G., et al. (2002), Kilimanjaro ice core records: Evidence of holocene climate change in tropical Africa, *Science*, *298*, 589–593.

Wagnon, P., P. Ribstein, B. Francou, and B. Pouyaud (1999a), Annual cycle of energy balance of Zongo Glacier, Cordillera Real, Bolivia, *J. Geophys. Res.*, *104*(D4), 3907–3923.

Wagnon, P., P. Ribstein, G. Kaser, and P. Berton (1999b), Energy balance and runoff seasonality of a Bolivian glacier, *Global Planet. Change*, *22*, 49–58.

Wagnon, P., P. Ribstein, B. Francou, and J. E. Sicart (2001), Anomalous heat and mass budget of Glaciar Zongo, Bolivia, during the 1997/98 El Niño year, *J. Glaciol.*, *47*, 21–28.

Wagnon, P., J. E. Sicart, E. Berthier, and J. P. Chazarin (2003), Wintertime high-altitude surface energy balance of a Bolivian glacier, Illimani, 6340 m above sea level, *J. Geophys. Res.*, *108*(D6), 4177, doi:10.1029/2002JD002088.

Waple, A. M., et al. (2002), Climate assessment for 2001, *Bull. Am. Meteorol. Soc.*, *83*, S1–S62.

D. R. Hardy, Morrill Science Center, Department of Geosciences, University of Massachusetts, 611 North Pleasant St., Amherst, MA 01003-9297, USA. (dhardy@geo.umass.edu)

T. Mölg, Tropical Glaciology Group, Department of Geography, Innsbruck University Network of Climate and Cryospheric Research (ICCR), University of Innsbruck, Innrain 52, A-6020 Innsbruck, Austria. (thomas.moelg@uibk.ac.at)